Kelvin-Helmholtz waves under southward interplanetary magnetic field

K.-J. Hwang,[1,2] M. M. Kuznetsova,[1] F. Sahraoui,[3] M. L. Goldstein,[1] E. Lee,[4] and G. K. Parks[5]

Received 22 February 2011; revised 26 April 2011; accepted 3 May 2011; published 5 August 2011.

[1] The Kelvin-Helmholtz waves have been observed along the Earth's low-latitude magnetopause and have been suggested to play a certain role in the entry of solar wind plasma into Earth's magnetosphere. In situ observations of the KH waves (KHW) and, in particular, a nonlinear stage of the KH instability, i.e., rolled-up KH vortices (KHVs), have been reported to occur preferentially for northward interplanetary magnetic field (IMF). Using Cluster data, we present the first in situ observation of nonlinearly developed KHW during southward IMF. The analysis reveals that there is a mixture of less-developed and more-developed KHW that shows inconsistent variations in scale size and the magnetic perturbations in the context of the expected evolution of KH structures. A coherence analysis implies that the observed KHW under southward IMF appear to be irregular and intermittent. These irregular and turbulent characteristics are more noticeable than previously reported KHW events that have been detected preferentially during northward IMF. This suggests that under southward IMF KHVs become easily irregular and temporally intermittent, which might explain the preferential in situ detection of KHVs when the IMF is northward. MHD simulation of the present event shows that during southward IMF dynamically active subsolar environments can cause KHV that evolve with considerable intermittency. The MHD simulations appear to reproduce well the qualitative features of the Cluster observations.

Citation: Hwang, K.-J., M. M. Kuznetsova, F. Sahraoui, M. L. Goldstein, E. Lee, and G. K. Parks (2011), Kelvin-Helmholtz waves under southward interplanetary magnetic field, *J. Geophys. Res.*, *116*, A08210, doi:10.1029/2011JA016596.

1. Introduction

[2] Understanding how the interaction of the solar wind (SW) with Earth's magnetosphere produces a transfer of plasma, momentum, and energy across the magnetopause is an important question in magnetospheric physics. Under southward interplanetary magnetic field (IMF), low-latitude dayside reconnection appears to be a dominant mechanism for SW transport, while under northward IMF, high-latitude reconnection and/or the onset of the Kelvin-Helmholtz instability (KHI) at the low-latitude boundary layer (LLBL) [*Eastman et al.*, 1976; *Mitchell et al.*, 1987] (also see reviews by *Lundin* [1988] and *Eastman* [2003]) appears to drive entry of solar wind plasma, energy, and momentum into the magnetosphere.

[3] The KHI is a well-known hydrodynamic instability that grows in the interface between two fluids that have a sufficient velocity difference. Since *Dungey* [1954] first suggested that the KHI might play an important role in the dynamics of Earth's LLBL between the fast magnetosheath flow and the relatively stagnant plasma sheet, the KH mode has generally been treated as a viscous interaction, which, however, cannot account for significant plasma transport.

[4] More recently, focus has shifted to a nonlinear stage of the KHI, i.e., *large-scale*, *rolled-up KH vortices* (KHVs) that facilitate SW entry into Earth's magnetosphere via 1) diffusive transport through the turbulent decay of KHVs whose onset has been attributed to a secondary KHI or Rayleigh-Taylor instability [*Nakamura et al.*, 2004; *Matsumoto and Hoshino*, 2004, 2006], 2) reconnection between stretched field lines due to the vortex motion [*Otto and Fairfield*, 2000; *Nykyri and Otto*, 2001; *Nakamura et al.*, 2006, 2008], or 3) kinetic Alfvén waves (KAW) through a mode conversion from KH surface waves [*Chaston et al.*, 2007]. These three processes can trigger plasma transport and mixing within or at the edge of rolled-up KHVs and are believed to play a crucial role in the evolution of the KHV structure, ultimately forming a broad mixing layer at Earth's dawn/

[1]NASA Goddard Space Flight Center, Greenbelt, Maryland, USA.
[2]Goddard Planetary and Heliophysics Institute, University of Maryland, Baltimore County, Baltimore, Maryland, USA.
[3]Laboratoire de Physique des Plasmas, CNRS-Ecole Polytechnique, Observatoire de Saint-Maur, Saint-Maur, France.
[4]School of Space Research, Kyung Hee University, Yongin, South Korea.
[5]Space Sciences Laboratory, University of California, Berkeley, California, USA.

0148-0227/11/2011JA016596

dusk flanks [*Mitchell et al.*, 1987; *Nakamura et al.*, 2006; *Hasegawa et al.*, 2009].

[5] The in situ observations of the nonlinear KH wave (KHW), i.e., rolled-up KHVs have been reported to occur preferentially for northward interplanetary magnetic field (IMF) [*Kivelson and Chen*, 1995; *Fujimoto et al.*, 2003; *Hasegawa et al.*, 2004], although a linear surface wave has been reported under southward IMF conditions [*Mozer et al.*, 1994; *Kawano et al.*, 1994]. Several explanations for this preference have been suggested, including: competition with a tearing mode that suppresses KHI development for large magnetic shear under southward IMF [*Chen et al.*, 1993, 1997; *Farrugia et al.*, 2003]; the formation of a slow rarefaction region with a magnetic pressure maximum just inside the magnetopause under southward IMF [*Miura*, 1995]; the formation of a thin KH-unstable plasma sheet layer between the northern and southern lobes during southward IMF that has a stabilizing effect on the KHI due to the intense lobe magnetic field [*Hashimoto and Fujimoto*, 2005]; and, during northward IMF, the formation of a dense LLBL resulting from high-latitude reconnection that lowers the threshold of the KHI, together with magnetosheath compressional waves that serve as seed fluctuations for the KHI during northward IMF [*Hasegawa et al.*, 2009].

[6] Studies of the competition between KH and tearing modes, however, found that KH modes dominate the tearing instability when the Alfvénic Mach number, M_A, associated with the velocity difference across the boundary layer is large, e.g., when $M_A > 1$ under no density gradient across the velocity shear layer [*Fuselier et al.*, 2000]. *La Belle-Hamer et al.* [1995] revealed that the threshold M_A for which tearing mode is quenched depends on the density ratio across the boundary layer.

[7] In this paper, we present first in situ observation of nonlinearly developed KHW during southward IMF. The data are from a Cluster crossing of the dawnside flank magnetopause on July 28, 2006. Based on the observation of both *less-developed* and *more-developed* KHW during a relatively short time period (~17 minutes) that shows dynamic variations in both scale sizes and fluctuation levels, as well as irregular variations in boundary-normal directions, we speculate that KH structures formed under southward IMF conditions are likely to become irregular (less coherent) and temporally intermittent. We suggest that those characteristics might explain the preferential detection of KHV under northward IMF. A global MHD simulation of the magnetosphere designed to mimic this event shows unstable and irregular structures of KHW together with a rapid evolution of the waves associated with the dynamically active environment that characterizes southward IMF. A "virtual" Cluster spacecraft flown through the simulation domain reproduces the quantitative features of the Cluster observation.

[8] In section 2, we present the overview of the event and estimate the evolutionary phases of KHW. In section 3, the intrinsic features of KHW under southward IMF are discussed using an analysis of scale sizes, magnetic fluctuations, and boundary normal directions. Deductions from this analysis are further supported by the comparison of the coherence of a series of KHW structures with a northward IMF KHV event. In section 4 we present the MHD simulation result for the present event, and conclude with a discussion.

2. Observations

2.1. Overview of the Event

[9] On July 28, 2006, Cluster-1 (C1), which was located near the magnetopause on the dawnside tail flank at [−13.1, −12.8, −3.2] Earth radii (R_E) in GSE coordinates, observed the repetitive patterns in the field and plasma signatures shown in Figure 1. The event occurred within a period of southward IMF (Figures 2a–2c, one minute resolution OMNI-HRO data from the ACE http://omniweb.gsfc.nasa.gov/ow_min.html). ACE was located near [225, −7, 20] R_E in GSE coordinates around/before the event. The ACE HRO data provide the time-shifted IMF and solar wind parameters at a model bow shock nose location [*Farris and Russell*, 1994] that varies with changes in solar wind conditions. We further time-shifted the HRO data to account for the shocked solar wind travel time to the location of C1, using the average velocity of the shocked solar wind measured by C1 when the spacecraft was located in the magnetosheath (~−538 km/s during 03:00–03:04 UT) and the distance between the model bow shock and the location of C1. This additional time shift is about 4.5 minutes and applied in Figure 2 where the event period is bounded by red vertical dashed lines. Note that it is ambiguous whether or not the observation shown in Figure 1 is the result of the local interaction between the shocked solar wind and the magnetosphere near the C1 location, or an evolved form of dayside magnetopause fluctuations that convect tailward along the magnetopause. (As discussed below, the surface waves have highly developed structures which implies the latter interpretation.) This ambiguity, together with uncertainties with the model used to map ACE data to the bow shock location, results in uncertainties in calculating the SW transit time from the bow shock nose to C1 location. These uncertainties make it difficult to accurately align beginning and end time of the solar wind time series with the C1 observation. Nevertheless, the error in a time shift would be an order of minutes, which still validates that the event occurred during mainly southward IMF conditions.

[10] Figure 1 shows the magnetic field (Figures 1a–1c); the magnetic field variation projected onto the xy_{GSE} plane (Figure 1d); the ion velocity, V_x (red), V_y (green), and V_z (blue) (Figure 1e); the ion density (Figure 1f); the ion (Figure 1g) and electron (Figure 1h) temperatures (see the caption for details). All parameters throughout this paper are shown in GSE coordinates. Multiple perturbations in B_z and changes in sign (Figure 1a) indicate that C1 encountered the magnetosheath plasma (negative B_z) and the magnetosphere plasma (positive B_z), repeatedly. Local processes, such as turbulent magnetosheath reconnection, might have given rise to these significant field fluctuations. However, the observed variations in plasma density and temperature support the interpretation that Cluster traveled between magnetosheath and magnetosphere repeatedly because positive (mostly negative) B_z periods are characterized by low (high) density (Figure 1f), and high (low) temperature (Figure 1g). Each of the repeated structures is separated by a rapid positive-to-negative change in B_z, as marked with vertical magenta

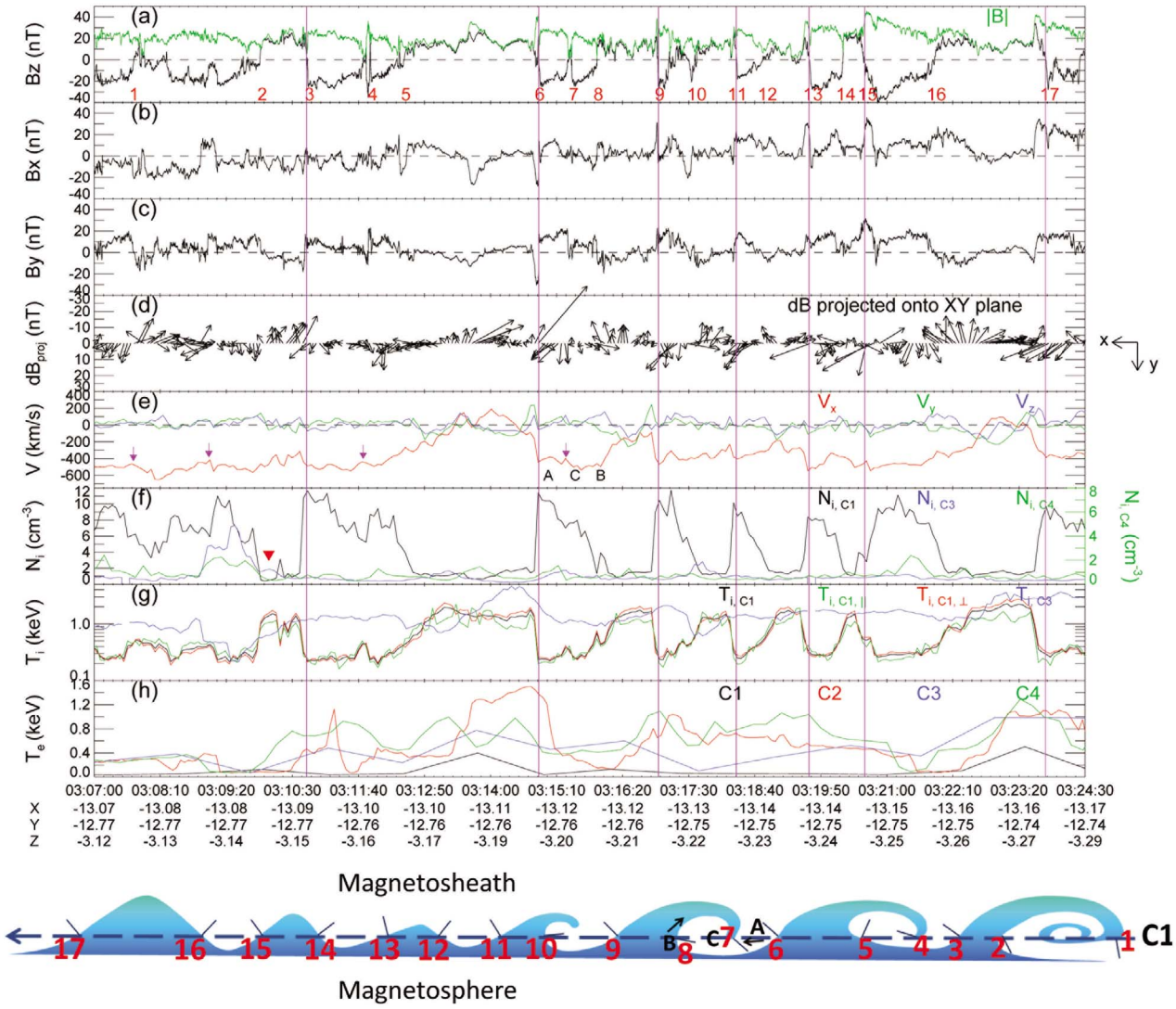

Figure 1. Observations from C1 during 2006-07-28/03:07:00–03:24:30 UT (all the parameters here and in Figures 2–9 are shown in GSE coordinates): (a) the z component (black) and the magnitude (green) of the magnetic field; (b and c) the x and y components of the magnetic field; (d) the magnetic field variation projected onto the xy plane; (e) the ion velocity, V_x (red), V_y (green), and V_z (blue); (f) the ion density measured by C1 (black), C3 (blue), and C4 (green); (g) the ion parallel (green), perpendicular (red), and total (black) temperature measured by C1, and the ion total temperature measured by C3 (blue); and (h) the electron temperature measured by C1 (black), C2 (red), C3 (blue), and C4 (green). These data come from the Flux Gate Magnetometer (FGM) experiment [*Balogh et al.*, 2001], the Plasma Electron And Current Experiment (PEACE) [*Johnstone et al.*, 1997], the Composition Ion Spectrometer (CIS) experiment [*Rème et al.*, 2001] (HIA for C1 and C3, and CODIF for C4), and the Spatio-Temporal Analysis of Field Fluctuations (STAFF) instrument [*Cornilleau-Wehrlin et al.*, 2003]. The vertical red lines demarcate seven consecutive KHV/KHW structures. At bottom is shown a cartoon representing C1 crossing of possible KHVs. The 17 boundaries between the magnetosheath and the magnetosphere, primarily determined by the B_z sign changes, are marked by red numbers, 1–17, in Figure 1a and the cartoon. A minimum variance analysis (MVA) of the magnetic field components is performed on each of these 17 boundaries, and projections of these boundary normals onto the xy plane are shown in the cartoon by dark blue lines. A red triangle in Figure 1f shows a time period where C3 located closest to Earth observed higher plasma density than that observed by C1 when a time delay associated with the C1-C3 separation along the wave propagation velocity has been taken into account.

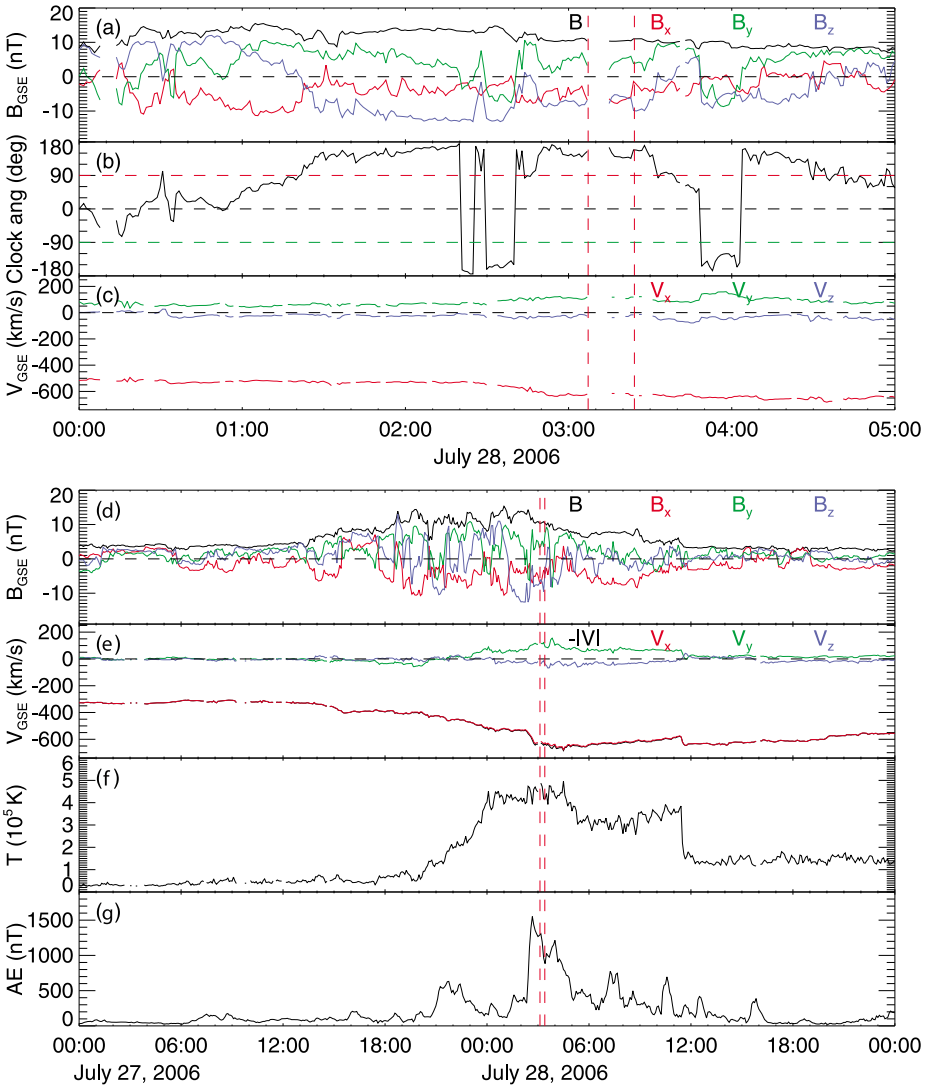

Figure 2. (a, b, and c) Five-hour-period solar wind parameters around the event from ACE High Resolution OMNI data at 1 minute resolution, after being time-shifted for the location of C1 as a reference. The event period is bounded by red dashed lines. (d-g) Two-day-period 1AU solar wind conditions around the event from ACE High Resolution OMNI data at 5 minute resolution. The event coincides near the peaks in the magnetosheath field magnitude (Figure 2a), solar wind velocity (Figure 2b) and temperature (Figure 2c), and AE index (Figure 2d) during southward IMF conditions (Figure 2a).

lines. Within each cycle, larger antisunward flow is observed during a mostly negative B_z period while slower, or even sunward flow is observed during a positive B_z period (Figure 1e). Particle energy spectrograms also distinguish the two distinct regions. Positive B_z regions in Figure 3a are populated by a large portion of higher-energy particles, while negative B_z regions by lower-energy particles (Figures 3b and 3d). This is more apparent for electrons (Figure 3b) than it is for ions (Figure 3d). Low-energy, parallel and/or antiparallel electron components are often clearly seen during a negative B_z period, while hotter, more isotropic distributions are noted during positive B_z (Figure 3c).

[11] All these signatures can be interpreted as repeated encounters by spacecraft with a cold, dense magnetosheath (with mostly negative B_z) and hot, tenuous magnetospheric (positive B_z) side near the flank of the magnetopause. Either surface waves (e.g., KHW) propagating along the magnetopause or a global inward-outward motion of the magnetopause (e.g., a breathing mode) [*Takahashi and Ukhorskiy*, 2007] can explain such repeating encounters by a spacecraft that is relatively stationary in space. In section 2.2 we identify vortical flow around the boundary coincidentally with densities that are the opposite of the normal expectation of lower density closer to Earth and higher density further away from Earth. From that analysis we conclude that the observations are indicative of surface waves rather than a bulk magnetosphere breathing motion.

2.2. Identification of KHW and Its Developed Waveform

[12] The first structure passed C1 at 03:07:00–03:10:44 UT (Figure 1) when C3 was located closer to the Earth than was

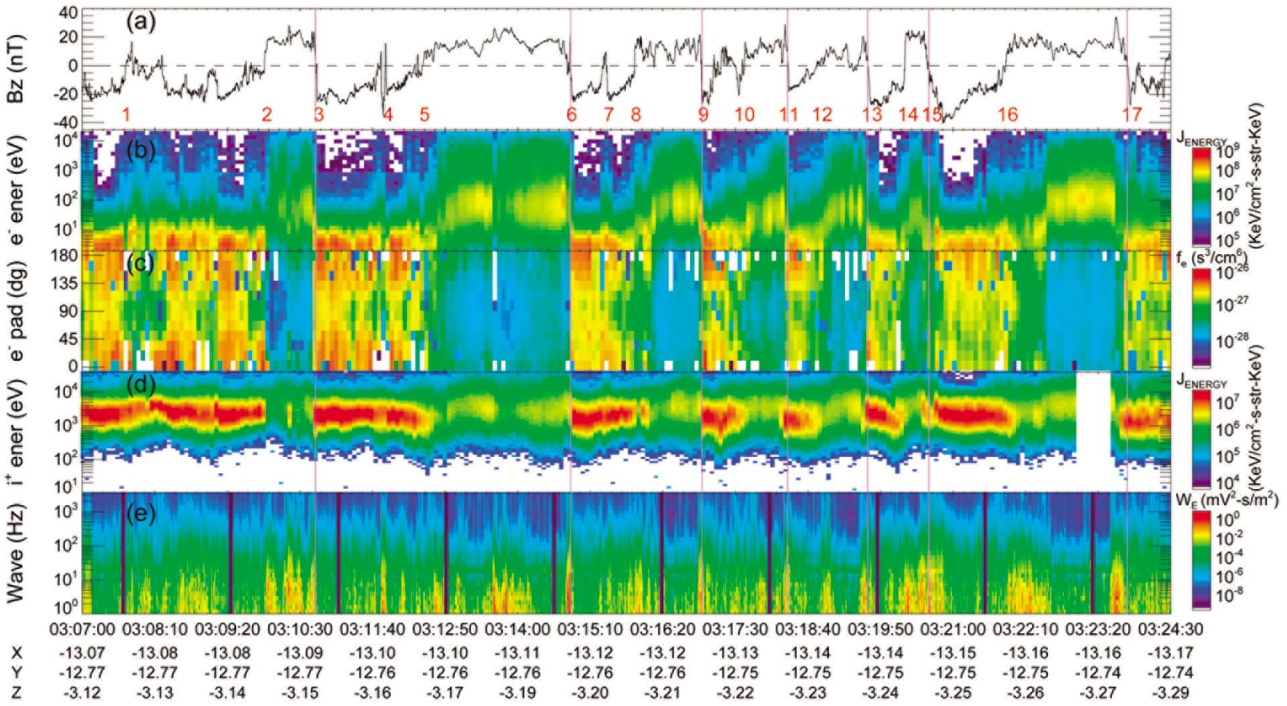

Figure 3. Particle and wave signatures observed by C1 during the same time period of Figure 1: (a) the *z* component of the magnetic field as reference; (b) the electron energy spectrogram; (c) the electron pitch angle distribution; (d) the ion energy spectrogram; and (e) the electric wave power spectral density. Seventeen boundaries are marked by red letters, 1 to 17, in Figure 3a.

C1 by ~1.2 R_E along the *y* direction. C3 traversed the outside of the magnetopause between ~03:08:50–03:10:20 UT as indicated by the ion density (blue line in Figure 1f), flow velocity, temperature, and particle energy spectrograms, all of which show magnetosheath features similar to those shown in Figures 1e and 1g and Figures 3b–3d from C1. Note that during the time period 03:09:54–03:10:14 UT, marked by a red triangle in Figure 1f, C3 (closer to Earth) observed higher plasma density than did C1 (further away from Earth), which is still valid when a time delay associated with the C1–C3 separation along the wave propagation velocity (see below) has been taken into account. C3 was located immediately outside of the magnetopause, or on the magnetosheath side of the boundary layer while C1 was on the magnetospheric side. This situation, which we call a *density reverse*, can arise if magnetosheath plasma is engulfed into the magnetosphere by nonlinear KHW [*Hasegawa et al.*, 2004]. Figure 4 shows the projections of the spacecraft locations relative to the center of Cluster tetrahedron, and variations of flow velocity during the $N_{i,C3} > N_{i,C1}$ interval onto the *xz* (Figure 4, left) and *xy* (Figure 4, right) planes.

[13] To see if vortical plasma flow is observed or not, flow vectors need to be viewed in the frame of the structure. Although other spacecraft (C2–C4), which mainly remained in the magnetosphere during the event as observed by C1, failed to detect similar repeated field signatures, they do show similar structures in density or/and temperature during the first and fourth structures shown in Figures 1f–1h. This might be explained by a boundary layer that has a finite thickness such that the outermost layer is subject to a process that changes the magnetic field properties (e.g., reconnection), but across which other plasma parameters change only gradually.

[14] We used the times that the four spacecraft passed the similar temperature profiles to derive the propagation velocity of the first KH structure. (Due to the different time resolution between the spacecraft for the PEACE three-dimensional distribution function data from which the electron temperature is calculated (see Figure 1h), we used the combination of the ion (for C1 and C3, Figure 1g) and electron (for C2 and C4, Figure 1h) temperatures.) These temperature profiles, however, show some differences in the duration of the structures and also differences in the detailed profiles, indicating a variation of the waveform across the boundary layer. In such cases the timings are determined based on the time shifts that give best correlations between any pair of spacecraft. Using these methods, we estimate the propagation velocities to be $(V_x, V_y, V_z)_{KH} = (-319.2, -12.9, 41.9)$ km/s for the first structure. The estimated propagation vector is shown in a gray arrow in Figure 4. (Note that the flow velocity is dominantly along the $-x$ direction (Figure 1e), suggesting that the wave vector would be mainly tailward, as derived from our timing analysis.)

[15] Using the estimated propagation velocity, we deduced flow vectors (in the rest frame of the structure—colored arrows in Figure 4) for the five consecutive time intervals from 03:09:54 to 03:10:14 UT (see the caption for details). When viewed from the north (looking down the *xy* plane (Figure 4, right)), a clockwise rotation inferred from each pair of the flow vectors at C1 and C3 corresponds well

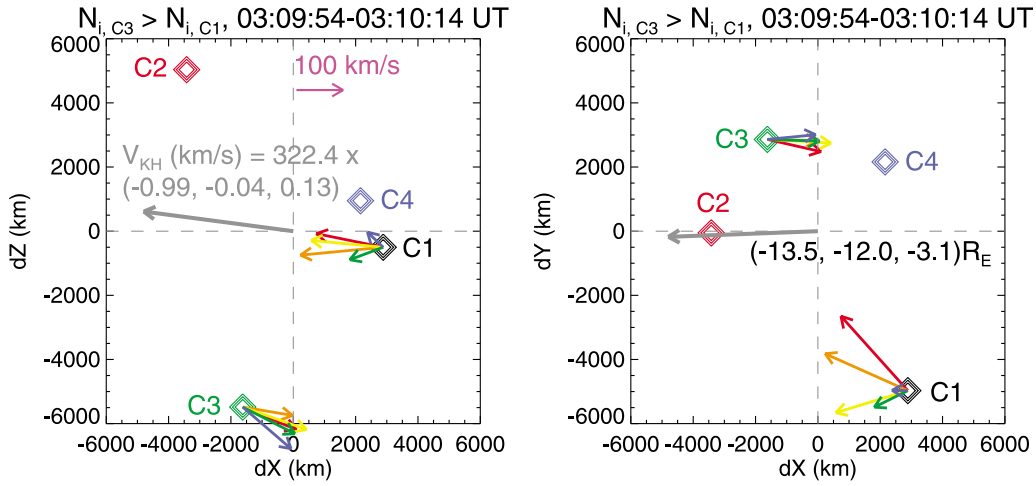

Figure 4. Locations of the four Cluster spacecraft in the (left) *xz* and (right) *xy* planes between 03:09:54–03:10:14 UT within the first structure. During this period, the plasma density observed by C3 (located closest to Earth) is higher than that observed by C1 (taking into account the time delay associated with the C1-C3 separation along the wave propagation velocity). The flow velocities observed at C1 and C3 have been transformed into the frame of the KHW, of which the relative velocity in GSE coordinates is determined by the four-spacecraft timing analysis (see the text). The projections of transformed flow vectors on the *xz* (Figure 4, left) and *xy* (Figure 4, right) planes during five consecutive spin periods (~4 seconds) are denoted by arrows with different colors (red arrows: 03:09:54–58 UT, orange: 03:09:58–03:10:02 UT, yellow: 03:10:02–06 UT, green: 03:10:06–10 UT, and blue: 03:10:10–14 UT). A magenta arrow corresponding to a flow speed of 100 km/s is shown in the top part of Figure 4 (left). Flow vectors in the *xy* plane demonstrate an expected clockwise vortical flow at the dawnside magnetopause, while those in the *xz* plane also indicate a vortical flow, but such that a helical structure might exist in three dimensions.

to the expected vortical streamline at the dawnside magnetopause. It is worth noting that the three-dimensional structure as evidenced by the flow velocities in the *xz* plane appear to create a helical motion.

[16] These simultaneous observations of vortical flow and the density reverse indicate that higher-density plasma (more-magnetosheath region) intruded into lower-density magnetospheric region as a result of the nonlinear evolution of KHW. Consequently, we conclude that the observed repetitive perturbations (Figure 1) represent surface waves propagating along the flank magnetopause, rather than a breathing mode of a global magnetospheric volume.

2.3. Different Evolutionary Phases of KHW

[17] Between 03:07:10–03:18:20 UT, each structure shows a short excursion to a positive B_z in the magnetosheath side (e.g., 03:07:41–03:08:18 UT for the first period, 03:11:43–52 UT for the second period, 03:15:20–27 UT for the third period, and around 03:17:21 UT for the fourth period as shown in Figure 1a). During these periods the plasma measurements (Figures 1f and 1g and Figures 3b and 3d) show intermediate signatures of magnetosheath and magnetosphere plasma, or a mixture of the two. Note that this positive-B_z excursion occurs near a halfway point of the magnetosheath-side passage by the spacecraft, and is not found during the following interval, 03:18:20–03:23:49 UT. These excursions can be interpreted as spacecraft crossings of a filamentary structure that contains magnetosheath plasma that has been energized during dayside reconnection, or, alternatively, is the leading edge of rolled-up KHVs, as illustrated at the bottom of Figure 1. (A series of the KH structures is drawn in the reverse order against the observed time series, as the most-tailward structure will be observed first by Cluster.) The engulfing/intruding, leading edge of KHW is evidence of a rolled-up KHV as a result of the nonlinear growth of KHW, and highly stretched field lines in the vortical structure can generate local filamentary structures, such as small-scale magnetic islands via reconnection [*Otto and Fairfield*, 2000; *Nykyri and Otto*, 2001; *Nakamura et al.*, 2008]. Therefore, the latter interpretation indicates that the observed KHW trains are in a different evolutionary state, separated out at ~03:18:20 UT. Another interpretation would be that the spacecraft trajectory moved slightly more in the magnetosphere during the later interval, 03:18:20–03:23:49 UT, compared to the earlier interval, 03:07:10–03:18:20 UT, and therefore, the leading edges of KHW could not be detected, as a result of a slow outward motion of the magnetopause. However, any noticeable changes in solar wind parameters that can cause the magnetopause to move outward are shown during the event. And, the differences found in following analyses and in the wavefront steepness (section 3) between the two intervals are hardly explained only by such spatial differences in the spacecraft trajectory. In the following we estimate the evolutionary phase of a train of KHWs.

[18] During the event period, the magnetic field measured by other spacecraft (C2–C4), which were closer to Earth than C1, did not show a noticeable periodicity or consistency with C1 observations. Figures 4c and 4d show that B_y becomes positive on the magnetosheath side, which corresponds to the spacecraft crossing near the northern edge of the KHW from a three-dimensional aspect of the KHW

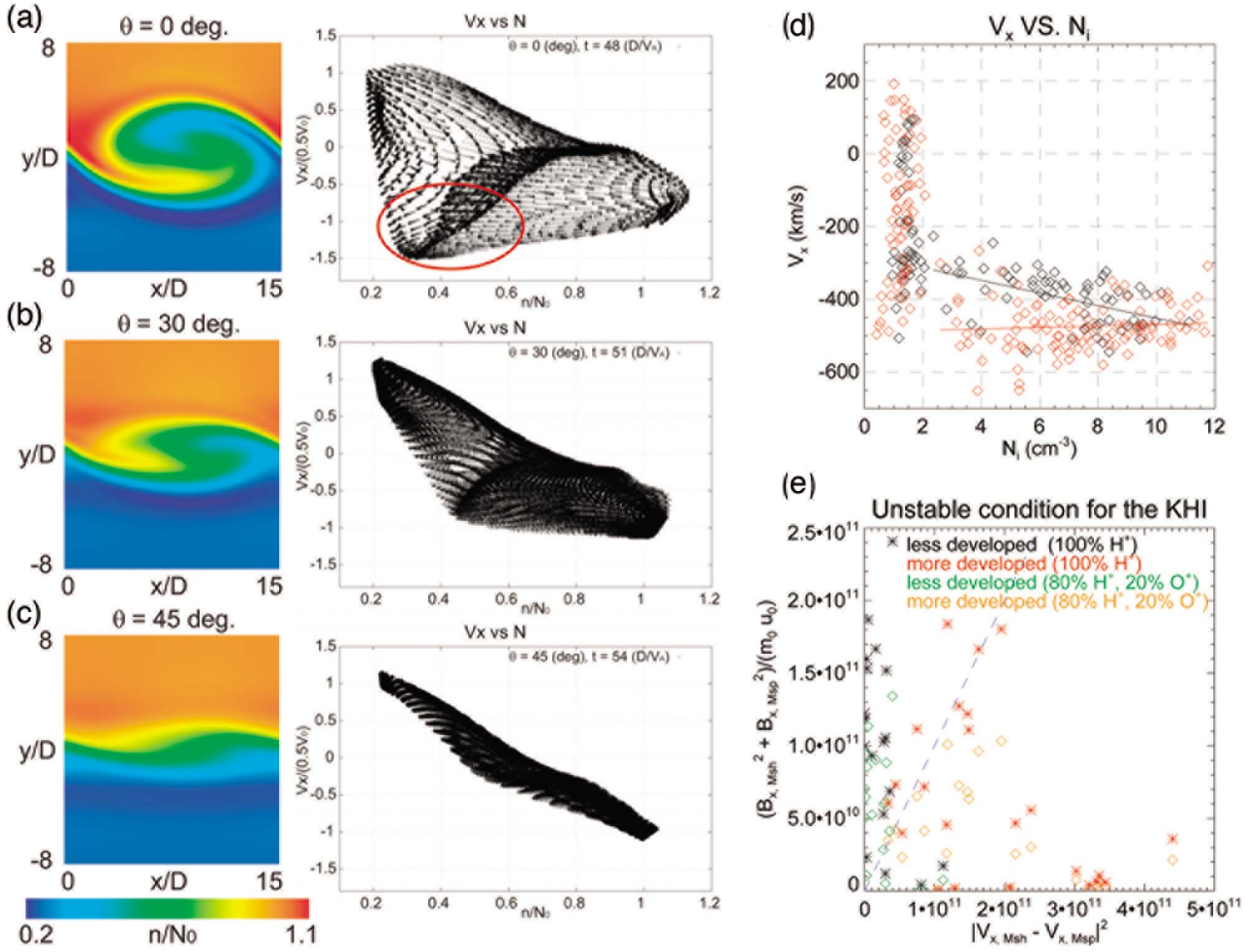

Figure 5. (a, b, and c) The degrees of the roll-up of KHV and V_x-N_i scatterplots, adopted from *Takagi et al.* [2006]. θ represents the angle that the magnetosheath field makes with respect to the magnetospheric field. (d) V_x-N_i distribution during 03:07:10–03:18:20 UT (red diamonds) and 03:18:20–03:23:49 UT (black diamonds) using measurements from C1. Linear fits for $N_i > 2$ cm^{-3} are overplotted for the two periods with a correlation coefficient of ~0.06 (red) and ~0.55 (black). (e) KHI-unstable condition for the two periods, 03:07:10–03:18:20 UT (red stars: 100\% H^+, orange diamonds: 20% O^+ assumed) and 03:18:20–03:23:49 UT (black stars: 100% H^+, green diamonds: 20% O^+ assumed).

structure, while B_y fluctuates around zero on the magnetospheric side. This, together with the failure to detect repetitive field structures by C2–C4, indicates that the spacecraft trajectory was located more toward the magnetospheric edge of the structure. For this (mainly) single-spacecraft detection of the KHW, the distribution of flow velocities (V_x) with respect to the ion density (N_i) suggests a clue as to whether the KHW is a linear surface wave or a nonlinear vortex.

[19] *Takagi et al.* [2006] and *Nakamura et al.* [2004] demonstrated in their simulations that at a certain radial distance from the center of a rolled-up vortex, the tenuous plasma sheet rotates faster than does the denser magnetosheath in response to an equal centrifugal force. Therefore, the low-density and faster-than-magnetosheath portion in V_x versus N_i distribution (the red circle in Figure 5a (right)) is evidence of a rolled-up vortex. This theoretical argument has been verified by *Hasegawa et al.* [2006] who used in situ data to show that only in the rolled-up vortices does the tailward speed of low-density, magnetospheric plasma exceed that of the magnetosheath.

[20] The V_x-N_i distribution for the present event is shown in Figure 5d. The lower-density, higher-velocity regime (e.g., $N_i < 7$ cm^{-3} and $V_x < -475$ km/s—threshold values chosen to represent a lower boundary of the nominal magnetosheath density and the nominal magnetosheath velocity, respectively) is dominated by the data obtained between 03:07:10–03:18:20 UT (red diamonds) rather than those measured between 03:18:20–03:23:49 UT (black). Note that the $V_x - N_i$ distribution is dependent on the spacecraft path relative to the vortex center. The circled area in Figure 5a (right) is most ideally obtained when the spacecraft traverses an outer part of a rolled-up KHV (the magnetosheath side from the vortex center). When the spacecraft traverses the inner region of a KHV (as suggested by the fact that a significant fraction of data points in Figure 5d shows $N_i <$ 2 cm^{-3}), the magnetospheric leading edge being rolled-up sunward results in a *smaller* tailward speed (see magenta

Table 1. The Normal Directions of 17 Boundaries, Indicated as 1 to 17 in Figure 1a, Calculated Using the Minimum Variance Analysis of the Magnetic Field Components[a]

	Normal	θ	ϕ
	More Developed		
1	(−0.13, 0.79, 0.60)	−81	37
2	(−0.35, 0.72, 0.59)	−64	36
3	(0.81, −0.58, −0.10)	144	−6
4	(0.92, −0.27, −0.29)	164	−17
5	(−0.19, −0.42, 0.89)	66	63
6	(0.74, −0.64, −0.22)	139	−13
7	(−0.75, 0.65, 0.13)	−41	7
8	(−0.73, 0.13, 0.67)	−10	42
9	(0.66, −0.65, −0.37)	135	−22
10	(−0.98, −0.11, −0.16)	6	−9
11	(0.51, −0.83, −0.22)	122	−13
	Less Developed		
12	(−0.61, −0.78, −0.13)	52	−7
13	(0.22, −0.97, −0.06)	103	−3
14	(−0.80, −0.60, 0.01)	37	1
15	(0.58, −0.81, 0.09)	126	5
16	(−0.68, −0.73, −0.05)	47	−3
17	(0.49, −0.86, −0.17)	120	−10

[a]The medium-to-minimum eigenvalue ratio in the minimum variance calculation is above 2.7. Angle θ characterizes the wavefront steepness in the xy plane, while angle ϕ the north-south deviation of the normal from the xy plane. Boundary normals are often deviated from the xy plane, which is prominently seen among the more-developed KHW boundaries (1–11).

arrows in Figure 1e that mark a reduced flow speed during positive- or almost zero–B_z intervals). Nevertheless, the overall distribution for $N_i > 2$ cm^{-3} in Figure 5d is different for the two time intervals: for 03:07:10–03:18:20 UT red diamonds are broadly distributed, similar to Figure 5a, and show a weak linearity with a correlation coefficient of ~0.06, The black diamonds (03:18:20–03:23:49 UT) reveal a better linear fit with a correlation coefficient of ~0.55 and their distribution is similar to that seen in Figure 5c.

[21] Note that during the third structure (03:14:40–03:16:58 UT) comparison of $V_{x,y}$ on the magnetosheath (A in Figure 1e and the cartoon) and on the magnetospheric (B) sides from a presumed vortex center (C) indicates vortical flow: $|V_x|_{atA} < |V_x|_{atB}$ but $|N_i|_{atA} > |N_i|_{atB}$. The black arrows in the cartoon represent flow velocity vectors in the frame of the KHW, i.e., when the average tailward propagation of the wave is subtracted. Figure 5d with specific observations of roll-up signatures (as described in section 2.2 and the preceding paragraph) implies that the KH structures detected between 03:07:10–03:18:20 UT might represent nonlinearly developed KHW. Based on these arguments, we refer to these KH structures at 03:07:10–03:18:20 UT and 03:18:20–03:23:49 UT as *more-developed* and *less-developed* KHW, respectively.

[22] Interestingly, the KH-unstable condition for incompressible plasmas [*Hasegawa*, 1975] using the plasma and field parameters obtained during 03:07:10–03:18:20 UT and 03:18:20–03:23:49 UT crossings, also sorts the two intervals, as shown in Figure 5e:

$$[\mathbf{B}Bk \cdot (v_2 - v_1)]^2 > \frac{1}{\mu_0}\left(\frac{1}{\rho_1} + \frac{1}{\rho_2}\right)\left[\mathbf{B}B(B_1 \cdot k)^2 + \mathbf{B}B(B_2 \cdot k)^2\right] \quad (1)$$

where $\mathbf{B}Bv_{1,2}$, $\rho_{1,2}$, and $\mathbf{B}BB_{1,2}$ represent flow velocity, plasma density, and magnetic field at sides 1 and 2, respectively. Here, the KH wave vector (**B** B k) was assumed to be directed to the $-x$ direction. The left-hand term in equation (1) is plotted in x, and the right-hand in y. The reference points were chosen to ensure that they were obtained near the interface of two velocity layers (near boundaries 3, 6, 9, 11, 13, 15, and 17, as denoted in Figure 1), but not immediately adjacent to the boundaries so as to exclude interference with possible microinstabilities. Multiple data points for each of these boundaries have been used with each pair of the magnetospheric and magnetosheath reference timings equally separated from the boundary so that the result is less affected by transient changes of the parameters based on a single data point per each boundary.

[23] Equation (1) assumes that the interface layer has no thickness and that there are abrupt jumps in physical quantities across the boundary in the magnetohydrodynamic (MHD) scale. Studies on KHI criterion including effects of boundary thickness have revealed that the thickness controls the growth rate and that finite thickness can lead to KHI-unstable configurations even when the inequality (1) is not satisfied [*Miura and Pritchett*, 1982; *Gratton et al.*, 2004]. *Gnavi et al.* [2006] also reported how sensitive the stability conditions of the supersonic MHD velocity shear layer (where compressibility can exert a considerable influence on the KH stability) are. Note that the velocity shear and magnetic field data used to test equation (1) are taken from near the magnetopause interface, where rapid changes in physical quantities are found with typical timescales ≤2 seconds (see Figure 1a, and also note that the resolution of the ion moments data in Figures 1e–1g is constrained by the spacecraft spin resolution, ~4 seconds). The estimated thickness of the interface (up to ~800 km from a roughly presumed upper limit of wave propagation speed of ~400 km/s) is an order of ion gyroradius (~300–400 km), and the velocity shear is mainly subsonic, or marginally supersonic ($0.4 < |v_2 - v_1|/C_s < 1.3$ where C_s is the sound speed) across the interface. Therefore, we continue adopting equation (1) to investigate the instability property, while clarifying that the result is useful to see whether the interface is currently unstable to the KHI, not to see whether the KHW is currently rolled up or not. The former, however, still provides a physical insight on the evolutionary phase of KHW between the two intervals.

[24] The data from 03:07:10–03:18:20 UT (red stars, Figure 5e) mostly satisfy the threshold condition for the nonlinear KHI, which becomes more evident when 20% of the magnetospheric plasma is assumed to be O^+ (orange diamonds), while the data from 03:18:20–03:23:49 UT (black stars) are mostly below the threshold even though 20% O^+ (green diamonds) is assumed. (Note that CIS-CODIF, mass-resolution data are not available for C1 during this event.) This indicates that the KH wavefronts observed during 03:07:10–03:18:20 UT are unstable to the KHI and can grow nonlinearly, while those observed during 03:18:20–03:23:49 UT appear to be linearly stable. If the KHW has already rolled up, then satisfying equation (1) implies that an interface within the vortex structure is itself unstable to a secondary KHI, which would lead to a turbulent decay of KHVs [*Nakamura et al.*, 2004; *Matsumoto and Hoshino*, 2004]. Such a cascade might explain the significant distor-

tion and irregularity of the boundary normal directions that were observed during the interval 03:07:10–03:18:20 UT (see Table 1).

3. KH Waves Under Southward IMF Conditions

[25] Equation (1) indicates that increases in velocity shear and plasma density, or a magnetic field perpendicular to the KH wave vector, lower the instability threshold with no preference for northward over southward IMF. However, observations of well-developed KHW during southward IMF are unusual. To investigate whether special solar wind conditions might have facilitated excitation of the KHI for this event, we show in Figures 2d–2g two days of solar wind data surrounding the event, marked by red dashed lines. The event roughly coincides with the peaks in the magnetic field magnitude, solar wind speed, and temperature, that are typical features of a solar wind corotating interaction region (CIR). This suggests that the CIR might have created favorable conditions for generating the observed KHW by creating a significant velocity shear across the magnetopause. Another factor facilitating the KHI development may be high O^+ levels in the magnetospheric density associated with enhanced ion outflow, plasmaspheric plumes, and/or substorm activity. As indicated in Figure 2g, AE peaked at the time of the event, which lowers the KHI threshold [*Bouhram et al.*, 2005].

[26] In the following we focus more on the characteristics (especially, irregular features) of the observed KHW under southward IMF with respect to their scale sizes (1), magnetic fluctuations (2), boundary normal directions (3), and the coherence of the KH structures (4).

[27] 1. The time interval of each structure passage in Figure 1 shows significant variation among the KH structures, suggesting that the period and wavelength of the observed KHW is irregular. Estimating the scale size from the duration of the passage of each structure is rather crude since it assumes that each of the structures has a relatively similar propagation velocity. Nonetheless, more-developed KH wave trains tend to have larger propagation speeds [*Belmont and Chanteur*, 1989] as has been shown from global MHD simulations [e.g., *Collado-Vega et al.*, 2007]. This yields larger scale size variations that would be indicated by duration of the passage of each individual structure. Moreover, more-developed KHW are, in general, expected to have larger sizes than less-developed ones as they grow nonlinearly with time. The sequence in Figure 1 tends to roughly follow that trend, but the last structure (03:20:37–03:23:49 UT) is apparently not well developed but is considerably larger than expected.

[28] 2. For the highly rolled-up KHVs, the in-plane components of the magnetic perturbations ($\sim\delta B_{xy}$ shown in Figure 1d) are also expected to be amplified while B_z is depleted [*Fairfield et al.*, 2000; *Otto and Fairfield*, 2000]. Such behavior is not apparent for this event. In particular, the two less-developed KH structures seen later (03:19:38–03:23:49 UT) have the largest magnetic fluctuation amplitudes. This indicates that all portions of the ~17 minute period that comprise the KHW train are not coherent; a situation that could be caused either by different excitation mechanism or varying evolutionary processes.

[29] 3. Table 1 shows the normal directions (n_x,n_y,n_z) of 17 boundaries, denoted in Figure 1a and the bottom cartoon. Projections of these boundary normals onto the *xy* plane have been used to construct the cartoon. The angle, $\theta = \arctan(n_y/n_x)$, $-180° < \theta \leq 180°$, defines the angle between the *xy* plane projections of the normals and the presumably tailward wave propagation direction. A positive (negative) θ indicates the normal points to the magnetosheath (magnetosphere) side, with $\theta = 0$ corresponding to the wavefront normal pointing to the wave propagation direction. This angle characterizes the wavefront steepness in the *xy* plane [*Foullon et al.*, 2008] (see the cartoon in Figure 1 where the *xy* plane projection of the normal is marked by a dark blue line at each boundary). The angle, $\phi = \arctan(n_z/\sqrt{(n_x^2 + n_y^2)})$ characterizes the north-south deviation of the normal from the *xy* plane. (Note that a positive (negative) ϕ indicates the normal pointing to the north (south).) For highly corrugated localized structures (e.g., boundaries along a highly developed KHV) the wavefront steepness might not show a consistent trend because it will depend sensitively on where on the boundary the spacecraft passes (e.g., this might be the case for the first and second KH structures). However, for the third and fourth structures during the more-developed interval, the wavefront steepness at the leading edge (boundaries, 8 and 10) is larger than that at the trailing edge (boundaries, 9 and 11). This pattern is less clear for the less-developed periods (boundaries 12–13, 14–15, and 16–17), as is expected for the KH structures that have different evolutionary phases because less-developed KHW are almost sinusoidal while nonlinearly growing KHW tend to further steepen at one edge (typically, at the leading edge [*Owen et al.*, 2004]. *Chen and Kivelson* [1993], however, reported a steeper KH wavefront at the trailing edge) than the other. More important is that boundary normals often deviate from the *xy* plane (Table 1). This is prominently seen among the more-developed KHW boundaries (1–11) and indicates that the observed KH structures have complicated three-dimensional topologies and that each structure has been differently distorted off from the mean boundary surface. If there were no significant temporal variations in the seed fluctuations for the KHI and no vortex deformation during convection, Cluster would be expected to observe a series of KH structures with relatively regular scale size, orientation, and fluctuation level for about ~17 minutes for the present event during which solar wind parameters did not vary significantly. Such behavior is not seen in Figure 1, all of which implies an irregular and temporally intermittent signature.

[30] The observed irregularities and inconsistent variations in the scale sizes (durations of the structure traverse by C1) and fluctuation levels of the KHW appear relatively more noticeable than those reported for northward IMF KHW events [*Chen and Kivelson*, 1993; *Kivelson and Chen*, 1995; *Fairfield et al.*, 2000; *Hasegawa et al.*, 2004; *Bouhram et al.*, 2005]. We continue this discussion using information on phase coherence of the time series magnetic field data for the northward/southward IMF KHW events (4).

[31] 4. The Fourier phases of a time series contain information of nonlinear (NL) interactions [*Theiler et al.*, 1992; *Hada et al.*, 2003; *Levrier et al.*, 2006], and can therefore provide insights into the nature of the turbulence (e.g., weak or strong, structurally intermittent or self-similar) [*Koga et al.*, 2007; *Sahraoui*, 2008]. To measure the strength of

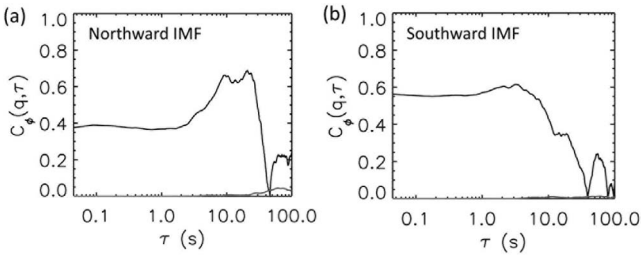

Figure 6. The coherence of the KHV structures (a) for the northward IMF event reported by *Hasegawa et al.* [2004] and (b) for the present event under southward IMF conditions.

NL effects in the observed KHW, or equivalently, to quantify the coherency of those waves, we use the technique of *surrogate data* developed by *Sahraoui* [2008]. This technique uses three time series data: the original (measured) magnetic field data B_O (t), and two surrogate (artificial) signals that have the same measured power spectra, but have random and coherent phases ($B_R(t)$ and $B_C(t)$, respectively). Comparison of three respective structure functions (SFs), defined by $S_{O,C,R}(q,\tau) = \sum_t |B_{O,C,R}(t+\tau) - B_{O,C,R}(t)|^q$ which is a function of q (the order of the SF) and τ (time increment), allows one to determine phase coherence, estimate its strength, and infer the timescale of the coherence [*Koga et al.*, 2007; *Sahraoui*, 2008]. A coherence index, $C_\phi(q,\tau)$ that measures the "relative distances" between the curves $S_{O,C,R}(q,\tau)$, is computed as a function of the time lag τ using the three SFs:

$$C_\phi(q,\tau) = \left(\frac{|S_O(\tau) - S_R(\tau)|}{|S_O(\tau) - S_R(\tau)| + |S_O(\tau) - S_C(\tau)|} \right)^{1/q} \quad (2)$$

Here we limit the study to the first-order SF, i.e., $q = 1$ (higher-order SFs show similar results). C_ϕ (τ) = 0 (1) means that phases are random (coherent), or equivalently, no strong nonlinearities are present [*Sahraoui*, 2008]. (Note that the second-order coherence index, $C_\phi(q = 2)$ is used to estimate the accuracy of the determination of the SFs [*Sahraoui*, 2008]: the results become unreliable if $C_\phi(q = 2)$ differs significantly from 0).

[32] Figure 6 compares the coherence of the structure function calculated from B_z profiles as observed during a ~16 minute period of the northward IMF event from *Hasegawa et al.* [2004] (Figure 6a), and the present event under southward IMF conditions (Figure 6b). $C_\phi(q = 1,2)$ is plotted in black and blue, respectively. (Other magnetic components, not shown, show similar features.) First we notice that both cases show a significant level of coherence ~0.7, confirming that strong nonlinear effects exist in the two KHW events. We also found that most of nonlinearity for the southward IMF event comes from the more-developed period when comparing the coherence level during the more- and less-developed periods, separately (not shown). This supports our conclusion that the KH waves are likely to be nonlinearly developed KHVs, especially during the more-developed interval.

[33] There are however differences between the two cases. For the southward IMF case (Figure 6b), the coherence increases as the scale τ decreases from $\tau \sim 30$ s to 3 s and remains constant for smaller scales. This can be interpreted as due to the intermittent nature of the turbulence down to $\tau \sim 3$ s. The turbulence then recovers its self-similar nature, meaning that structures are present at all scales (in other words, the system becomes globally scale-invariant), which is consistent with the "classical" image of turbulence [*Frisch*, 1995]. For the northward IMF case (Figure 6a), the coherence level after reaching its maximum at ~20 s decreases at smaller scales. This supports the idea of a dominance of particular coherent structures at a certain scale (or equivalently, the global scale invariance breaks at that scale), and that smaller scales have a more random (or wavelike) nature [*Sahraoui et al.*, 2009]. These differences indicate that the KHVs under northward IMF conditions contain more coherent and regular structures at a particular scale. In contrast, the southward IMF KHVs appear to be less coherent or more irregular.

[34] Note that the northward IMF event [*Hasegawa et al.*, 2004] occurred on the dusk flank close to the dayside terminator ($x = \sim -3$ R_E), as opposed to the present southward IMF event that was detected at the dawnside tail flank. Such a difference in the observation location might have contributed the observed differences in the coherence properties to some extent. However, a northward IMF KHW event that was detected at even further tailward on the dawn flank by ISEE 2 (at ~[−17, −14, 5]R_E) [*Chen and Kivelson*, 1993] shows a noticeable periodicity and regularity during the time period of ~30 minutes, indicating the trend that came from the above phase-coherence comparison.

4. MHD Simulation Results of the Cluster Observations

[35] The coherence analysis in section 3 implies that the observed KHW under southward IMF appear to be irregular (less coherent) and turbulent. These irregular characteristics are more noticeable than previously reported KHW/KHV events that have been detected during northward IMF. This might be related to the intrinsic nature of the magnetopause behavior under different IMF conditions. The driving factor for the observed irregularity can result from temporal variations in the seed fluctuations for the KHI near the subsolar magnetopause (remote origin), or, vortex deformation during tailward convection due to external effects (local origin). We expand on this idea using a three-dimensional MHD simulation that models the Cluster observations.

[36] Figures 7 and 8 show the results of a simulation using the BATS-R-US code run for our parameters at the CCMC (Community Coordinated Modeling Center, http://ccmc.gsfc.nasa.gov). The grid in the xy plane cut used for the simulation (shown in Figure 7f) is designed to resolve the dynamics and physical processes occurring at the dayside/subsolar region and flank magnetopause. We have zoomed into the region of the dawnside magnetopause between $-16 \le x(R_E) \le 0$ and $-16 \le y(R_E) \le -8$). In Figures 7a–7e, the current density is color-coded and the flow velocities are indicated by arrows.

[37] Figures 7a–7c manifest rapid and dynamic evolution of KH structures during southward IMF (between 02:18:00–02:26:00 UT in Figures 2a–2c): the flow vortex associated with the surface undulations ($-8.5 \le x(R_E) \le -5$ and $-12 \le y(R_E) \le -10.4$ in Figure 7a) indicates that the fluctuations

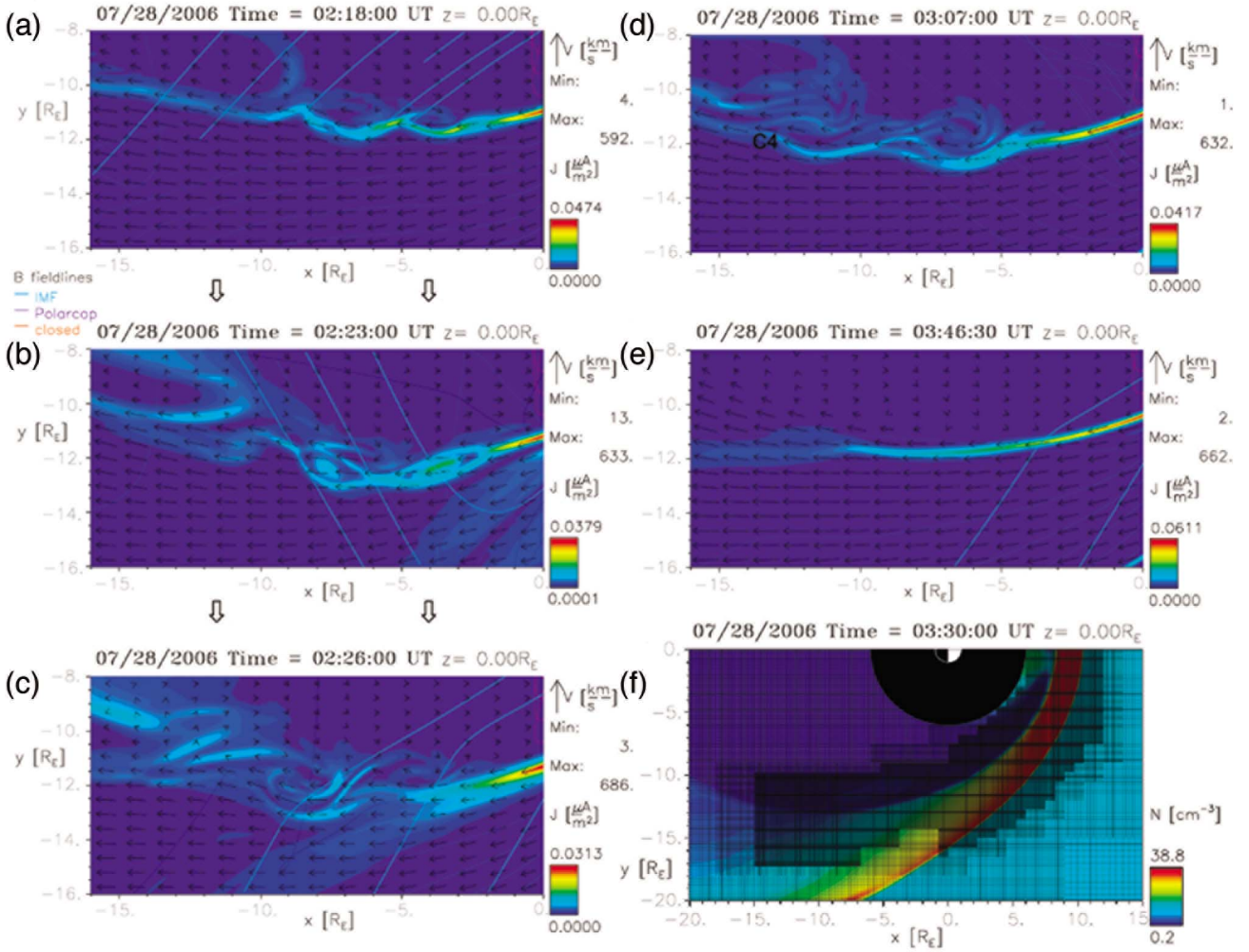

Figure 7. MHD simulation for the Cluster observation using the BATS-R-US code. (a–e) The region of the dawnside flank magnetopause is blown up ($-16 \le x(R_E) \le 0$ and $-16 \le y(R_E) \le -8$), the current density is color-coded, and flow velocities are denoted by arrows. (f) The grid in the *xy* plane used for the simulation.

are the developed KH mode. Two FTE-like structures that have been generated at the dayside magnetopause and propagate tailward along the magnetopause faster than the KHW ($-8.5 \le x(R_E) \le -2$ and $-13.2 \le y(R_E) \le -11.5$, Figure 7b) results in the KH structures into a turbulent and irregular state (Figure 7c). In contrast, the flank magnetopause under northward IMF at 03:46:30 UT (Figure 7e) forms as a stable boundary with no prominent KH activity. Note that the IMF clock angle is ~50° at 03:46:30 UT, which might have suppressed the development of the KHI mode, or delocalized the source region of the KHI generation [*Farrugia et al.*, 1998].

[38] To see if such FTEs on the boundaries of KHWs driven under southward IMF conditions are observed, we investigated the geometry of KHW boundaries observed by C1 using a minimum variance analysis (MVA) of the magnetic field components. B_{lmn} components for boundary 2 (denoted in Figure 1a) and the cartoon) are presented in Figure 8). The maximum B_m observed coincidentally with the B_l reversal indicates a typical FTE structure, as illustrated on the right side. We observed a variety of magnetic geometries along the KHW boundaries, and the magnetic geometries that can be interpreted as a FTE or magnetic island are observed only among the *more-developed* KHW boundaries. This is consistent with our simulation results as well as previously reported simulations [*Nakamura et al.*, 2008].

[39] Figure 7d, captured at 03:07:00 UT, corresponding to the Cluster observation time, depicts clear vortical flows (around $x = -6.5$ R_E and $y = -11.3$ R_E). Multiple current

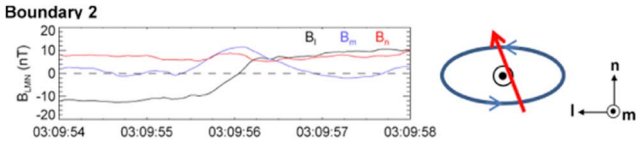

Figure 8. For boundary 2 denoted in Figure 1a and the cartoon, the magnetic field components are transformed in the LMN coordinates system using a minimum variance analysis. A possible magnetic geometry is illustrated on the right.

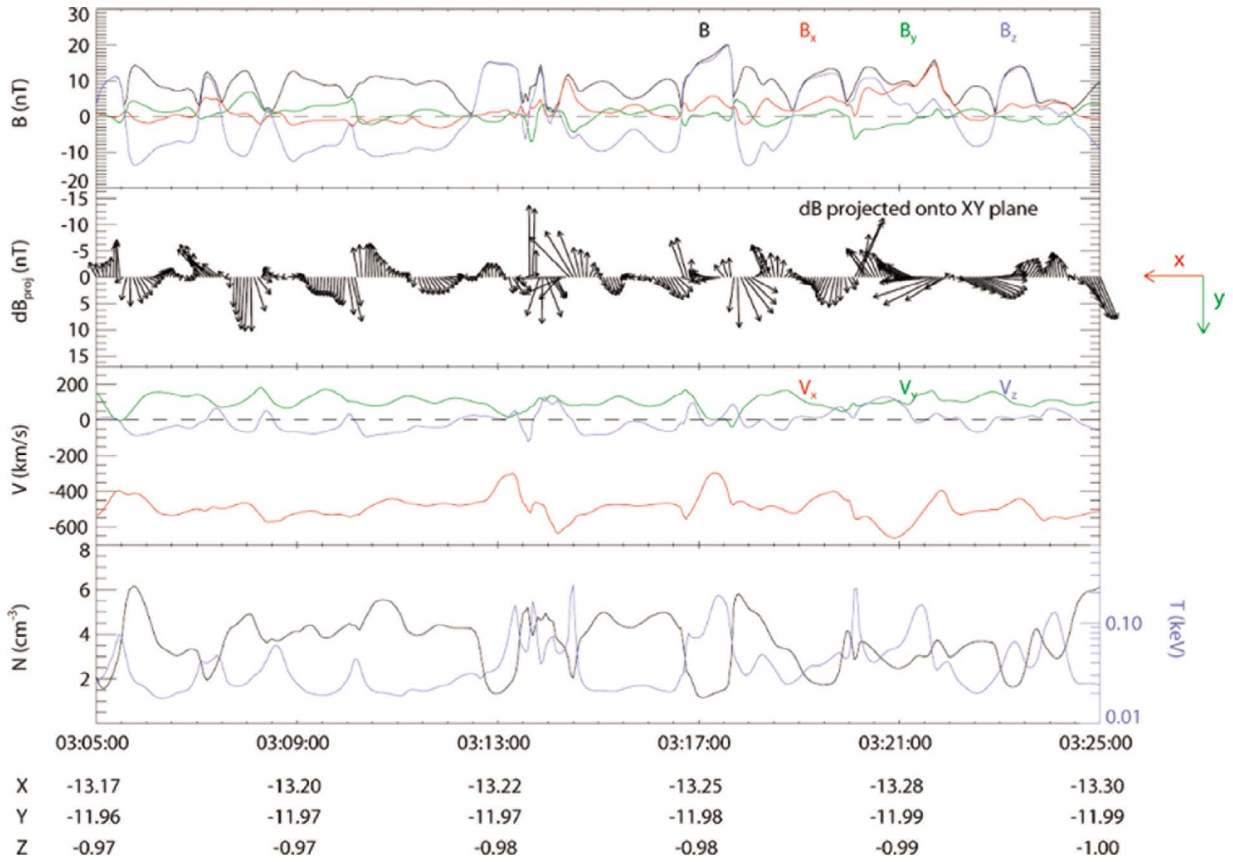

Figure 9. The observation from the virtual spacecraft "C4" that has been flown in the simulation domain nearly at the time of Figure 7d where the location of "virtual C4" is shown: the magnetic field, B (black), B_x (red), B_y (green), and B_z (blue); the magnetic field variation projected onto the xy plane; the plasma velocity, V_x (red), V_y (green), and V_z (blue); the plasma density (black), and temperature (blue).

layers within the vortex imply that the waves were already well developed. Among four "virtual" Cluster spacecraft flown in the simulation domain, "virtual C4" best reproduces the in situ Cluster observations qualitatively, as is found from the comparison of Figure 9 to Figure 1: B_z profile that shows a short $|B_z|$ dip in the magnetosheath side, magnetic field fluctuations in the xy plane, reduced antisunward flow in the positive B_z crossings, and the anticorrelation between plasma density and temperature. A series of six KH structures (compared to seven repetitive structures shown in Figure 1) show different periods and different scale sizes rather than periodic and regular patterns. Their scale sizes (as small as ~2.3 R_E and up to 7.0 R_E) are smaller than the estimated scale sizes deduced from C1 observations (Figure 1e).

[40] Our simulation results can be compared with the previous simulations of the KHW under purely southward IMF conditions reported by *Claudepierre et al.* [2008]. They found two outer and inner KH modes propagating tailward along the magnetopause boundary and the inner edge of the boundary layer, respectively, fairly monochromatic vortical structures of the KHWs, and the interaction between the inner and outer KH modes leading to a coupled oscillation of the LLBL. Our MHD simulations do not show such a two wave structure. Note that *Claudepierre et al.* [2008] used the LFM (Lyon-Fedder-Mobarry) global, three-dimensional code under uniform solar wind conditions with a different solar wind driving velocity for each independent run. Such uniform conditions could have suppressed the generation of FTEs at the dayside magnetopause, which, in turn, leads to rather monochromatic wavelengths of the KHWs.

5. Discussion and Conclusions

[41] The Cluster spacecraft observed a series of both more-developed and less-developed KHW during ~17 minutes at the dawnside tail magnetopause under southward IMF conditions. The variations in scale size, magnetic perturbations, and boundary normal directions of the KHW do not always show a consistent trend in the context of the expected evolution of KH structures. The coherence analysis implies that the observed KHW under southward IMF appear to be irregular (less coherent) and turbulent.

[42] The results of the MHD simulation that models the Cluster event show that under southward IMF, the KHVs that develop along the flank magnetopause tend to become unstable due to both (remote) subsolar fluctuations, and (local) direct interactions with external dynamics, such as FTEs that have been generated near the subsolar location and that drift along the magnetopause to the magnetotail, disrupting the previously formed KHVs. This might explain

the preferential detection of KHVs during northward IMF for which the development of KHV is rather stationary, and the structures are long-lasting [*Kuznetsova et al.*, 2008]. Southward IMF conditions typically generate dynamically active subsolar behavior that gives rise to temporally intermittent and irregular signatures in vortex formation and evolution. Such evolution would leave little chance to observe well-developed KHW under southward IMF.

[43] The observation of KHVs and the behavior of the flank magnetopause during varying IMF conditions reported by *Nykyri et al.* [2006], and the observation of KHVs associated with FTEs as interpreted by *Kivelson and Chen* [1995], supports this speculation. A statistical study made by *Collado-Vega et al.* [2007] using the simulated MHD data driven by real solar wind conditions also supports our conclusion. They reported that the KH vortices generated under southward IMF were less ordered. However, a statistical study of in situ observations of KHW classified by northward and southward IMF conditions is needed before definitive conclusions can be reached.

[44] **Acknowledgments.** This study was supported, in part, by NASA's Cluster mission and, in part, by a Magnetospheric Multiscale Interdisciplinary Science grant at the Goddard Space Flight Center and by Goddard grant 67394324/NCC5-494 to the UMBC/GEST program. We acknowledge all Cluster instrument teams, including PEACE, CIS, STAFF, and FGM staffs and the Cluster Active Archive (http://caa.estec.esa.int/caa) from which all the processed science-level data were downloaded except the CIS data. Simulation results have been provided by the Community Coordinated Modeling Center at Goddard Space Flight Center through their public Runs on Request system (http://ccmc.gsfc.nasa.gov). K.-J. Hwang appreciates helpful advice from Hiroshi Hasegawa.

[45] Philippa Browning thanks Scott Boardsen and Fausto Gratton for their assistance in evaluating this paper.

References

Balogh, A. C., et al. (2001), The Cluster magnetic field investigation: Overview of in-flight performance and initial results, *Ann. Geophys.*, *19*, 1207.

Belmont, G., and G. Chanteur (1989), Advances in magnetopause Kelvin-Helmholtz instability studies, *Phys. Scr.*, *40*, 124.

Bouhram, M., B. Klecker, G. Paschmann, S. Haaland, H. Hasegawa, A. Blagau, H. Rème, J.-A. Sauvaud, L. M. Kistler, and A. Balogh (2005), Survey of energetic O^+ ions near the dayside mid-latitude magnetopause with Cluster, *Ann. Geophys.*, *23*, 1281.

Chaston, C. C., M. Wilber, F. S. Mozer, M. Fujimoto, M. L. Goldstein, M. Acuña, H. Rème, and A. Fazakerley (2007), Mode conversion and anomalous transport in Kelvin-Helmholtz vortices and kinetic Alfvén waves at the Earth's magnetopause, *Phys. Rev. Lett.*, *99*, 175004, doi:10.1103/PhysRevLett.99.175004.

Chen, Q., A. Otto, and L. C. Lee (1997), Tearing instability, Kelvin-Helmholtz instability, and magnetic reconnection, *J. Geophys. Res.*, *102*, 151.

Chen, S. H., and M. G. Kivelson (1993), Nonsinusoidal waves at the magnetopause, *Geophys. Res. Lett.*, 20, 2699.

Chen, S. H., M. G. Kivelson, J. T. Gosling, R. T. Walker, and A. J. Lazarus (1993), Anomalous aspects of magnetosheath flow and of the shape and oscillations of the magnetopause during an interval of strongly northward interplanetary magnetic field, *J. Geophys. Res.*, *98*, 5727.

Claudepierre, S. G., S. R. Elkington, and M. Wiltberger (2008), Solar wind driving of magnetospheric ULF waves: Pulsations driven by velocity shear at the magnetopause, *J. Geophys. Res.*, *113*, A05218, doi:10.1029/2007JA012890.

Collado-Vega, Y. M., R. L. Kessel, X. Shao, and R. A. Boller (2007), MHD flow visualization of magnetopause boundary region vortices observed during high-speed streams, *J. Geophys. Res.*, *112*, A06213, doi:10.1029/2006JA012104.

Cornilleau-Wehrlin, N., et al. (2003), First results obtained by the Cluster STAFF experiment, *Ann. Geophys.*, *21*, 437.

Dungey, J. W. (1954), Electrodynamics of the outer atmosphere, in *Physics of the Ionosphere: Report of the Conference Held at the Cavendish Laboratory, Cambridge, September*, p. 229, Phys. Soc. of London, London.

Eastman, T. E. (2003), Historical review (pre-1980) of magnetospheric boundary layers and the low-latitude boundary layers, in *Earth's Low-Latitude Boundary Layer*, *Geophys. Monogr. Ser.*, vol. 133, edited by P. T. Newell and T. Onsager, p. 1, AGU, Washington, D. C.

Eastman, T. E., E. W. Hones, S. J. Bame, and J. R. Asbridge (1976), The magnetospheric boundary layer: Site of plasma, momentum and energy transfer from the magnetosheath into the magnetosphere, *Geophys. Res. Lett.*, *3*, 685–688.

Fairfield, D. H., A. Otto, and T. M. et al (2000), Geotail observations of the Kelvin-Helmholtz instability at the equatorial magnetotail boundary for parallel northward fields, *J. Geophys. Res.*, *105*, 21,159.

Farris, M. H., and C. T. Russell (1994), Determining the standoff distance of the bow shock: Mach number dependence and use of models, *J. Geophys. Res.*, *99*, 17,681.

Farrugia, C. J., F. T. Gratton, L. Bender, H. K. Biermat, N. V. Erkaev, J. M. Quinn, R. B. Torbert, and V. Dennisenko (1998), Charts of joint Kelvin-Helmholtz and Rayleigh-Taylor instabilities at the dayside magnetopause for strongly northward interplanetary magnetic field, *J. Geophys. Res.*, *103*, 6703.

Farrugia, C. J., F. T. Gratton, R. B. Torbert, L. Bender, G. Gnavi, K. W. Ogilvie, N. V. Erkaev, R. P. Lepping, and P. Stauning (2003), On the dependence of dayside kelvin-helmholtz activity on imf orientation, *Adv. Space Res.*, *31*, 1105.

Foullon, C., C. J. Farrugia, A. N. Fazakerley, C. J. Owen, F. T. Gratton, and R. B. Torbert (2008), Evolution of Kelvin-Helmholtz activity on the dusk flank magnetopause, *J. Geophys. Res.*, *113*, A11203, doi:10.1029/2008JA013175.

Frisch, U. (1995), *Turbulence*, Cambridge Univ. Press, Cambridge, U. K.

Fujimoto, M., T. Tonooka, and T. Mukai (2003), Vortex-like fluctuations in the magnetotail flanks and their possible roles in plasma transport, in *Earth's Low-Latitude Boundary Layer*, *Geophys. Monogr. Ser.*, vol. 133, edited by P. T. Newell and T. Onsager, p. 241, AGU, Washington, D. C.

Fuselier, S. A., S. M. Petrinec, and K. J. Trattner (2000), Stability of high-latitude reconnection site for steady northward imf, *Geophys. Res. Lett.*, *27*, 473.

Gnavi, G., F. T. Gratton, C. J. Farrugia, and L. Bilbao (2006), The KH stability of the supersonic magnetopause flanks modeled by continuous profiles for the transition, in *Plasma and Fusion Science: 16th IAEA Technical Meeting on Research Using Small Fusion Devices*, edited by J. Julio and E. Herrera Velazquea, *AIP Conf. Proc.*, 875, 296–299.

Gratton, F. T., L. Bender, C. J. Farrugia, and G. Gnavi (2004), Concerning a problem on the Kelvin-Helmholtz stability of the thin magnetopause, *J. Geophys. Res.*, *109*, A04211, doi:10.1029/2003JA010146.

Hada, T., D. Koga, and E. Yamamoto (2003), Phase coherence of MHD waves in the solar wind, *Space Sci. Rev.*, *107*, 463.

Hasegawa, A. (1975), *Plasma Instabilities and Non-linear Effects*, Springer-Verlag, New York.

Hasegawa, H., M. Fujimoto, T.-D. Phan, H. Rème, A. Balogh, M. W. Dunlop, C. Hashimoto, and R. TanDokoro (2004), Transport of solar wind into Earth's magnetosphere through rolled-up Kelvin-Helmholtz vortices, *Nature*, *430*, 755.

Hasegawa, H., M. Fujimoto, K. Takagi, Y. Saito, T. Mukai, and H. Rème (2006), Single-spacecraft detection of rolled-up Kelvin-Helmholtz vortices at the flank magnetopause, *J. Geophys. Res.*, *111*, A09203, doi:10.1029/2006JA011728.

Hasegawa, H., et al. (2009), Kelvin-Helmholtz waves at the Earth's magnetopause: Multiscale development and associated reconnection, *J. Geophys. Res.*, *114*, A12207, doi:10.1029/2009JA014042.

Hashimoto, C., and M. Fujimoto (2005), Kelvin-Helmholtz instability in an unstable layer of finite thickness, *Adv. Space Res.*, *37*, 527.

Johnstone, A. D., et al. (1997), PEACE: A Plasma Electron And Current Experiment, *Space Sci. Rev.*, *79*, 351.

Kawano, H., S. Kokubun, Y. Yamamoto, K. Tsuruda, H. Hayakawa, M. Nakamura, T. Okada, A. Matsuoka, and A. Nishida (1994), Magnetopause characteristics during a four-hour interval of multiple crossings observed with GEOTAIL, *Geophys. Res. Lett.*, *21*, 2895.

Kivelson, M. G., and S.-H. Chen (1995), The magnetopause: Surface waves and instabilities and their possible dynamic consequences, in *Physics of the Magnetopause*, *Geophys. Monogr. Ser.*, vol. 90, edited by P. Song, B. U. Ö. Sonnerup, and M. F. Thomsen, p. 257, AGU, Washington, D. C.

Koga, D., A. C.-L. Chian, R. A. Miranda, and E. L. Rempel (2007), Intermittent nature of solar wind turbulence near the Earth's bow shock: Phase coherence and non-Gaussianity, *Phys. Rev. E*, *75*, 046401, doi:10.1103/PhysRevE.75.046401.

Kuznetsova, M., M. Hesse, D. Sibeck, L. Rastaetter, G. Toth, and T. Gombosi (2008), Non-steady reconnection in global simulations of

magnetosphere dynamics, *Eos Trans. AGU*, *89*(53), Fall Meet. Suppl., Abstract SM23C-04.

La Belle-Hamer, A. L., A. Otto, and L. C. Lee (1995), Magnetic reconnection in the presence of sheared flow and density asymmetry: Applications to the Earth's magnetopause, *J. Geophys. Res.*, *100*, 11,875.

Levrier, F., E. Falgarone, and F. Viallefond (2006), Fourier phase analysis in radio-interferometry, *Astron. Astrophys.*, *456*, 205.

Lundin, R. (1988), On the magnetospheric boundary layer and solar wind energy transfer into the magnetopause, *Space Sci. Rev.*, *48*, 263.

Matsumoto, Y., and M. Hoshino (2004), Onset of turbulence induced by a Kelvin-Helmholtz vortex, *Geophys. Res. Lett.*, *31*, L02807, doi:10.1029/2003GL018195.

Matsumoto, Y., and M. Hoshino (2006), Turbulent mixing and transport of collisionless plasmas across a stratified velocity shear layer, *J. Geophys. Res.*, *111*, A05213, doi:10.1029/2004JA010988.

Mitchell, D., F. Kutchko, D. Williams, T. Eastman, L. Frank, and C. Russell (1987), An extended study of the low-latitude boundary layer on the dawn and dusk flanks of the magnetosphere, *J. Geophys. Res.*, *92*, 7394.

Miura, A. (1995), Dependence of the magnetopause Kelvin-Helmholtz instability on the orientation of the magnetosheath magnetic field, *Geophys. Res. Lett.*, *22*, 2993.

Miura, A., and P. L. Pritchett (1982), Nonlocal stability analysis of the MHD Kelvin-Helmholtz instability in a compressible plasma, *J. Geophys. Res.*, *87*, 7431.

Mozer, F. S., H. Hayakawa, S. Kokubun, M. Nakamura, T. Okada, T. Yamamoto, and K. Tsuruda (1994), The morningside low-latitude boundary layer as determined from electric and magnetic field measurements on geotail, *Geophys. Res. Lett.*, *21*, 2983.

Nakamura, T. K. M., D. Hayashi, M. Fujimoto, and I. Shinohara (2004), Decay of MHD-scale Kelvin-Helmholtz vortices mediated by parasitic electron dynamics, *Phys. Rev. Lett.*, *92*, 145001, doi:10.1103/PhysRevLett.92.145001.

Nakamura, T. K. M., M. Fujimoto, and A. Otto (2006), Magnetic reconnection induced by weak Kelvin-Helmholtz instability and the formation of the low-latitude boundary layer, *Geophys. Res. Lett.*, *33*, L14106, doi:10.1029/2006GL026318.

Nakamura, T. K. M., M. Fujimoto, and A. Otto (2008), Structure of an MHD-scale Kelvin-Helmholtz vortex: Two-dimensional two-fluid simulations including finite electron inertial effects, *J. Geophys. Res.*, *113*, A09204, doi:10.1029/2007JA012803.

Nykyri, K., and A. Otto (2001), Plasma transport at the magnetospheric boundary due to reconnection in Kelvin-Helmholtz vortices, *Geophys. Res. Lett.*, *28*, 3565.

Nykyri, K., A. Otto, B. Lavraud, C. Mouikis, L. M. Kistler, A. Balogh, and H. Rème (2006), Cluster observations of reconnection due to the Kelvin-Helmholtz instability at the dawnside magnetospheric flank, *Ann. Geophys.*, *24*, 2619.

Otto, A., and D. H. Fairfield (2000), Kelvin-Helmholtz instability at the magnetotail boundary: MHD simulation and comparison with Geotail observations, *J. Geophys. Res.*, *105*, 21,175.

Owen, C. J., M. G. G. T. Taylor, I. C. Krauklis, A. N. Fazakerley, M. W. Dunlop, and J. M. Bosqued (2004), Cluster observations of surface waves on the dawn flank magnetopause, *Ann. Geophys.*, *22*, 971.

Rème, H., et al. (2001), First multispacecraft ion measurements in and near the Earth's magnetosphere with the identical Cluster ion spectrometry (CIS) experiment, *Ann. Geophys.*, *19*, 1303.

Sahraoui, F. (2008), Diagnosis of magnetic structures and intermittency in space-plasma turbulence using the technique of surrogate data, *Phys. Rev. E*, *78*, 026402, doi:10.1103/PhysRevE.78.026402.

Sahraoui, F., M. L. Goldstein, P. Robert, and Y. V. Khotyaintsev (2009), Evidence of a cascade and dissipation of solar-wind turbulence at the electron gyroscale, *Phys. Rev. Lett.*, *102*, 231102, doi:10.1103/PhysRevLett.102.231102.

Takagi, K., C. Hashimoto, H. Hasegawa, M. Fujimoto, and R. TanDokoro (2006), Kelvin-Helmholtz instability in a magnetotail flank-like geometry: Three-dimensional MHD simulations, *J. Geophys. Res.*, *111*, A08202, doi:10.1029/2006JA011631.

Takahashi, K., and A. Y. Ukhorskiy (2007), Solar wind control of Pc5 pulsation power at geosynchronous orbit, *J. Geophys. Res.*, *112*, A11205, doi:10.1029/2007JA012483.

Theiler, J., S. Eubank, A. Longtin, B. Galdrikian, and J. D. Farmer (1992), Testing for nonlinearity in time series: the method of surrogate data, *Physica D*, *58*, 751.

M. L. Goldstein, K.-J. Hwang, and M. M. Kuznetsova, NASA Goddard Laboratory Space Flight Center, Greenbelt, MD 20771, USA. (melvyn.l.goldstein@nasa.gov; Kyoung-Joo.Hwang@nasa.gov; Maria.M.Kuznetsova@nasa.gov)

E. Lee, School of Space Research, Kyung Hee University, Yongin, Gyeonggi 446-701, South Korea. (eslee@khu.ac.kr)

G. K. Parks, Space Sciences Laboratory, University of California, Berkeley, CA 94720, USA. (parks@ssl.berkeley.edu)

F. Sahraoui, Laboratoire de Physique des Plasmas, CNRS-Ecole Polytechnique, Observatoire de Saint-Maur, F-94107 Saint-Maur, France. (fouad.sahraoui@lpp.polytechnique.fr)